Olefins from Natural Gas by Oxychlorination

Author(s):
Zichittella, Guido; Aellen, Nicolas; Paunović, Vladimir; Amrute, Amol P.; Pérez-Ramírez, Javier

Olefins from Natural Gas via Oxychlorination Catalysis

Guido Zichittella, Nicolas Aellen, Vladimir Paunović, Amol P. Amrute, and Javier Pérez-Ramírez*

Abstract: Ethylene and propylene are the key building blocks of the chemical industry, but current processes are unable to close the growing gap between demand and manufacture. Herein, we report an exceptional europium oxychloride (EuOCl) catalyst for the selective (≥95%) production of light olefins from ethane and propane *via* oxychlorination chemistry, achieving yields of ethylene (90%) and propylene (40%) unparalleled by any existing olefin production technology. The outstanding performance was rationalized by its bifunctional character, integrating the alkane oxychlorination into alkyl chloride and its dehydrochlorination into the olefin, thus recycling the halogen source. Moreover, EuOCl is able to process mixtures of methane, ethane, and propane to produce the olefins, thereby reducing separation costs of the alkanes in natural gas. Finally, the EuOCl catalyst was scaled up in technical form, which preserves the outstanding performance for >150 h under realistic process conditions.

Figure 1. Closed-loop chlorine-mediated process for the one-step conversion of abundant light alkanes to valuable ethylene and propylene, which are the main building blocks of the chemical industry. An optimal catalytic material for this process should integrate the ability to functionalize the alkane into the corresponding alkyl chloride and to dehydrochlorinate the latter to yield an olefin, enabling the full recycle of the halogen source.

Vast conventional and unconventional natural gas reserves are rich in ethane and propane, offering a great potential as feedstock to produce ethylene and propylene, the platform molecules for the manufacture of virtually all polymers, pharmaceuticals, and chemicals.[1] Currently, these olefins are produced *via* steam-cracking, fluid-catalytic cracking, and/or catalytic dehydrogenation, which are highly capital- and energy-intensive and are unable to close the growing gap between their demand and manufacture.[1b,2] Thus, the replacement of these highly endothermic technologies with one-step, exothermic processes would result in enormous economic benefits.[2c,3] In this direction, the oxidative dehydrogenation of ethane and propane,[2a,4a] the partial oxidation of ethane,[4b,c] and the oxidative coupling of methane[4d] have been extensively studied for decades as a way to attain olefins, but so far they have failed to reach commercial reality due to the lack of suitable catalysts that can achieve economically attractive yields of ethylene and propylene (<75% and 30%, respectively). The catalytic alkane oxychlorination route, comprising the reaction of an alkane with hydrogen chloride (HCl) and oxygen, is appealing as it enables to selectively functionalize the alkane under moderate conditions.[1a,5] However, so far this route has mainly targeted the production of vinyl chloride monomer or alkyl chloride, where ethylene or propylene was observed as a by-product with low yields of 50% or 20%, respectively.[1a,6] The selective production of ethylene and propylene in a single step from the corresponding alkane would be highly appealing. This requires the design of a multifunctional catalytic material that can

integrate the oxychlorination of the alkane to the alkyl chloride, followed by its dehydrochlorination to yield the olefin (**Figure 1**).

In our quest for a novel multifunctional catalytic active phase, we have investigated the gas-phase oxychlorination of ethane and propane under variable conditions over different catalytic families, including: cerium oxide (CeO_2), vanadyl pyrophosphate ($(VO)_2P_2O_7$), titanium oxide (TiO_2), iron phosphate ($FePO_4$), and europium oxychloride (EuOCl). The catalysts were compared by evaluating the product distribution obtained in the oxychlorination of ethane and propane at *ca.* 20% and 15% alkane conversion, respectively (**Figure 2a** and **b**; Supporting Information, **Figure S1**), obtained by adjusting the reaction temperature measure in the center of the catalyst bed. Based on this rationale, the catalysts can be classified into three different groups. The first category is represented by CeO_2, which led to the lowest yields of olefin due to the formation of chlorinated hydrocarbons and combustion products in EOC and particularly POC. The second class, represented by $(VO)_2P_2O_7$ and TiO_2, achieved high yields of ethylene (with 80% and 90% selectivity in EOC, respectively), however, caused pronounced formation of combustion products in POC. Finally, $FePO_4$ and EuOCl enabled to reach over 95% selectivity to alkene in both EOC and POC. EuOCl displayed the highest yields of ethylene and propylene at unaltered selectivity (*vide infra* **Figure 3c**; Supporting Information, **Figure S4c**), thus emerging as an outstanding catalyst for olefin production *via* oxychlorination chemistry. Our recent studies have uncovered europium oxychloride as exceptional catalyst for ethylene oxychlorination to vinyl chloride monomer,[7a] and europium oxybromide for methane oxybromination to methyl bromide and HBr oxidation to Br_2,[7b] testifying the relevance of Eu-based catalysts for hydrocarbon upgrading and halogen looping. X-ray diffraction (XRD) and N_2 sorption analyses of the materials before to and after catalytic tests showed no alterations of the crystallographic structure, but evidenced a small decrease in the total surface area (Supporting Information, **Figure S2**). We have assessed

[*]   G. Zichittella, N. Aellen, V. Paunović, Dr. A. P. Amrute, Prof. J. Pérez-Ramírez
       Institute for Chemical and Bioengineering
       Department of Chemistry and Applied Biosciences, ETH Zurich
       Vladimir-Prelog-Weg 1, 8093 Zurich, Switzerland
   E-mail: jpr@chem.ethz.ch

       Supporting information for this article is given via a link at the end of the document.

the stability of this promising active phase, and demonstrated its robustness in preserving the outstanding performance for over 100 h on stream in both EOC and POC (Supporting Information, **Figure S3a** and **b**). The XRD analysis of the samples collected after the run indicated no alternation of the bulk structure (Supporting Information, **Figure S3c**) while a slight increase in the crystallinity of the sample was evidenced from high resolution transmission electron microscopy (HRTEM) and by a small drop in the total surface (Supporting Information, **Figure S3c** and **d**). We sampled the materials after 5 h on stream in both EOC and POC and confirmed that the surface area (8 $m^2 g^{-1}$ in both cases) stabilizes after few hours on stream. Thermodynamic calculations show that the transformation of EuOCl to EuCl$_3$ is highly unfavored in the operating conditions of the oxychlorination reaction (Supporting Information, **Figure S3e**), which might be due to its structural arrangement, alternating halide and oxide layers, as shown in **Figure 1**. Finally, we have conducted elemental analysis on the used catalyst and confirmed the absence of coke deposits (Supporting Information, **Table S4**).

Further evaluation of EuOCl under variable conditions

showed the preservation of high selectivity (>90%) in a wide range of temperatures (623-847 K), and feed concentration of alkanes (1.5-6 vol.%), O_2 (3-6 vol.%), and HCl (1-15 vol.%) (**Figure 2c** and **d**), highlighting the robustness of EuOCl in both reactions. The formation of alkenes might in principle come from the oxidative dehydrogenation of the alkane over the catalyst. Thus, to demonstrate the pivotal role HCl in the feed in alkane activation and olefin generation, a test was performed in the absence of HCl. Both the alkane conversions and alkene selectivities were drastically dropped (**Figure 2c** and **d**). Interestingly, by switching from 0 vol.% to 1 vol.% of HCl, the alkane conversion and particularly olefin selectivity were boosted in both alkane oxychlorination reactions. Further optimization of the alkane inlet concentrations enabled the attainment of the highest single-pass yields of ethylene and propylene (90% and 40%, respectively) among any alkane-to-olefins upgrading route (**Figure 2c** and **d**).

Olefin production from alkane *via* oxychlorination chemistry stem from integration of alkane oxychlorination to produce alkyl chloride and subsequent dehydrochlorinated of the latter to yield the corresponding alkene on the catalyst surface (*vide supra*
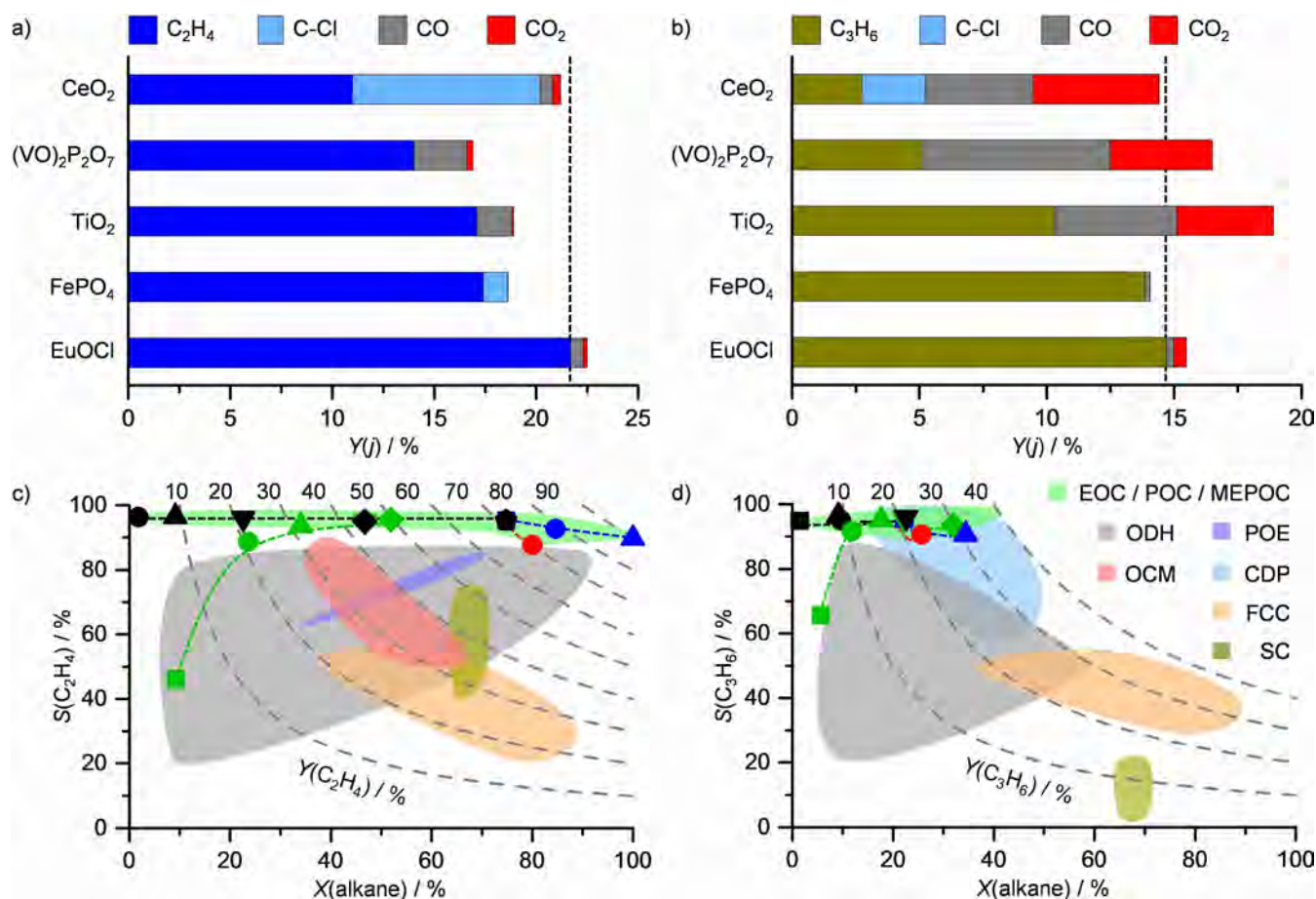
Figure 2. Catalytic performance expressed as single-pass yield of products (Y(j)) in the oxychlorination of a) ethane (EOC) and b) propane (POC) at ca. 20% and 15% alkane conversion, respectively, and alkene selectivity *versus* alkane conversion over EuOCl in c) EOC and d) POC at variable conditions. EuOCl represents a superior catalyst for both reactions, leading to the highest yield of olefins (dashed lines in a) and b)). Conditions: alkane-based GHSV = 155-415 h^{-1} (details in Supporting Information, **Table S3**). .EuOCl was further studied in c) EOC and d) POC at variable temperature (black) and feed concentration of HCl (green), O$_2$ (red), and alkane (blue) (details of symbols in Supporting Information, **Table S2**). The dashed gray lines indicate the olefin yield, whereas the colored areas denote the alkane conversion and olefin selectivity achievable in the oxychlorination of light alkanes and their mixtures over EuOCl (EOC, POC, MEPOC; green; *vide infra* Supporting Information, **Figure S5**), oxidative dehydrogenation of ethane and propane (ODH; gray),[2a,4a] partial oxidation of ethane (POE; blue),[4b,c] oxidative coupling of methane (OCM; red),[4d] catalytic dehydrogenation of propane (CDP; light blue),[1b] fluid catalytic cracking (FCC; orange)[8a] and steam cracking (SC; yellow)[8b] of ethane and naphtha. All results are expressed on a molar basis.
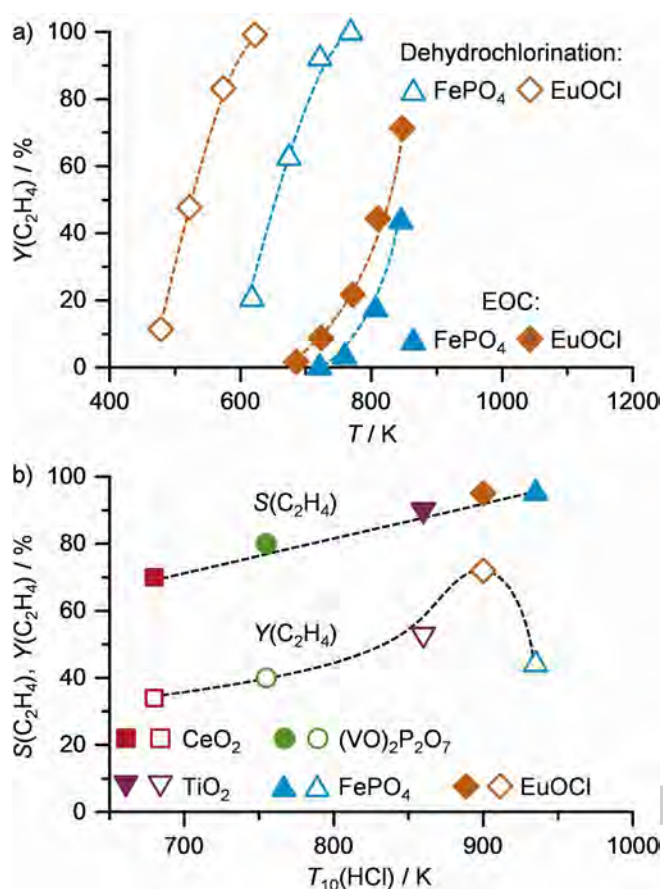
Figure 3. a) Yields of ethylene *versus* temperature in C_2H_5Cl dehydrochlorination (open symbols) and in EOC (solid symbols) over EuOCl (orange) and FePO$_4$ (blue). b) Selectivity (solid symbols) and yield (open symbols) of ethylene in EOC *versus* the oxidizing ability of the catalyst under typical oxychlorination conditions (T_{10}(HCl)). The latter is measured as the temperature to attain 10% HCl conversion in the gas-phase HCl oxidation to Cl$_2$ (Supporting Information, Figure S4a).

Figure 1). Nonetheless, these chloro-derivatives were not observed over EuOCl (*vide supra* **Figure 2a** and **b**; Supporting Information, **Figure 1**), which might be explained by its fast dehydrochlorination kinetic. To confirm this, we performed ethyl chloride and propyl chloride dehydrochlorination experiments on EuOCl and FePO$_4$ and observed that ethylene and propylene generation occurred at much lower temperature compared to EOC and POC, particularly in the case of EuOCl (**Figure 3a**; Supporting Information, **Figure S4b**).

To rationalize the different performance of the catalysts in EOC and POC, the gas-phase HCl oxidation to Cl$_2$ was studied (Supporting Information, **Figure S4a**) and taken as a relative measure of the oxidizing ability of the catalysts under typical oxychlorination conditions. Thus, if the temperature at which *ca.* 10% HCl conversion is attained in HCl oxidation, T_{10}(HCl), is high, the material possesses a low oxidizing character. This temperature was found to correlate linearly with olefin selectivity in EOC and POC (**Figure 3b**; Supporting Information, **Figure S4c**), suggesting that the systems with lower reducibility are preferred to achieve a high olefin selectivity, as a likely consequence of the suppressed combustion reactions as evidenced in the case of EuOCl and FePO$_4$ (*vide supra* **Figure 2a** and **b**). However, if the reducibility is too low, the
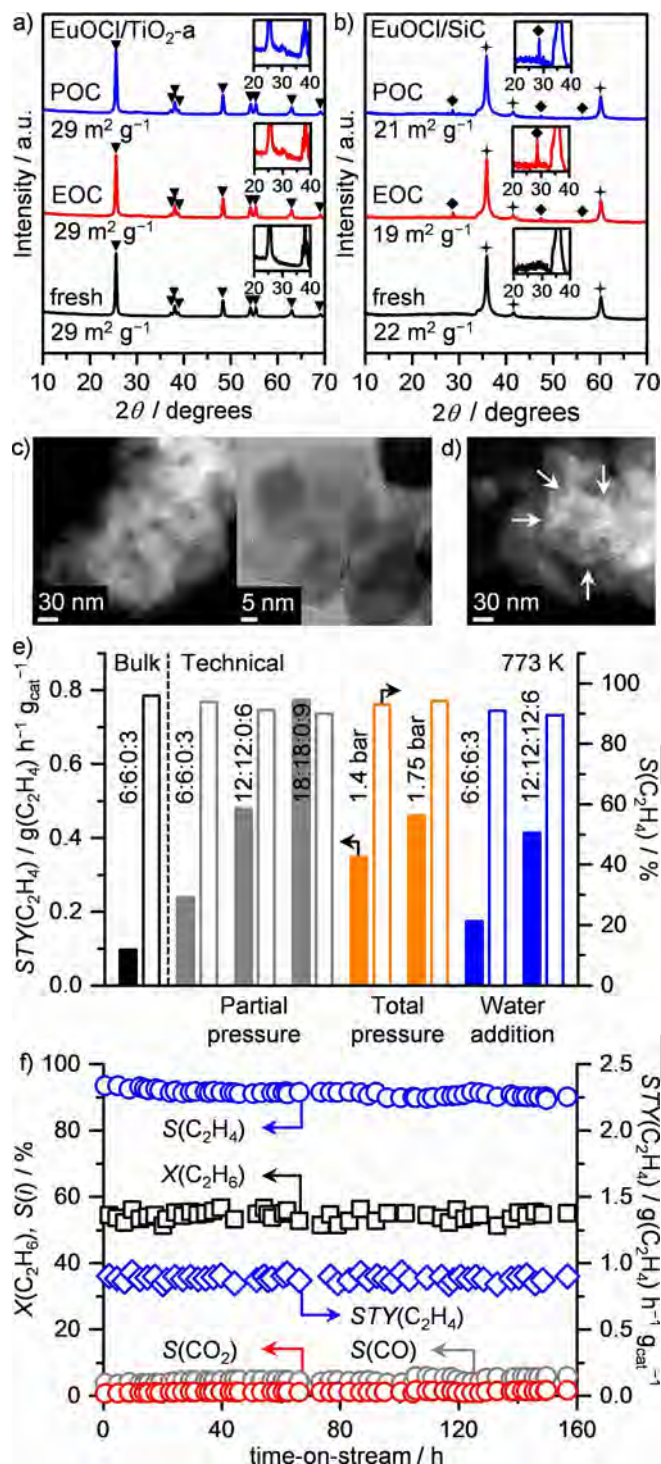
olefin yield can be lowered as seen for FePO$_4$. EuOCl appeared to have the optimal oxidizing potential, as it achieves the highest yields of olefins in both EOC and POC (**Figure 3b**; Supporting Information, **Figure S4c**). Thus, the outstanding performance of EuOCl can be rationalized by its balanced redox properties, enabling it to selectively functionalize the alkane and suppress undesired reactions, and its unpaired ability to readily dehydrochlorinate the produced alkyl chloride, allowing it to selectively yield olefins and to recycle the halogen source (Supporting Information, **Figure S5b** and **c**).

Due to the increasing scarceness of oil reserves, the world is currently undergoing an unprecedented revolution in raw hydrocarbons feedstock supply, with vast natural gas being the leading flag.[9] Consequently, we explored the potential of EuOCl in the oxychlorination of mixtures of methane, ethane, and propane (MEPOC) (Supporting Information, **Figure S5d** to **g**) to show the level of flexibility of this catalytic technology with respect to the feed composition. In this reaction, the onset temperature for propylene formation was lower than the one for ethylene, in line with the higher activity observed in POC than EOC. At 773 K, 20% and 27% yield of ethylene and propylene were achieved at >95% selectivity (Supporting Information, **Figure S5d**). Methane conversion and CO$_x$ formation were negligible (<5%). Moreover, we have investigated the effect of increased feed concentration of HCl and varying reactants ratio on the catalytic performance (Supporting Information, **Figure S5e** to **g**), which show that the yields of ethylene and propylene could be improved to 30% and 40%, respectively, at >95% selectivity. In this respect, the olefins mixture could then potentially be upgraded by known technologies to gasoline blends over zeolite- or supported metal-based systems.[10] These results show an attractive feature of the EuOCl catalyst preserving the high alkene selectivity even in the alkane mixture, which gives an extra-potential for natural gas upgrading due to its low sensitivity to feed purity.

To demonstrate the practical potential of EuOCl-based system for olefin production, we developed a technical catalyst by dispersing europium (10 wt.%) onto millimeter-sized bodies of silicon carbide (SiC), silicon oxide (SiO$_2$), zirconium oxide (ZrO$_2$), and titanium oxide anatase (TiO$_2$-a). Evaluation of these systems in EOC and POC identified EuOCl/TiO$_2$-a as the best catalyst for ethylene production, enabling unaltered ethylene selectivity and higher ethane conversion compared to bulk EuOCl, and EuOCl/SiC as the best system for propylene production, maintaining >90% propylene selectivity and reaching 40% propylene yield (Supporting Information, **Figure S6**). This suggests that the carrier selection plays an important role in controlling the performance of the EuOCl phase. We performed XRD analysis of the best ethylene and propylene generators before and after the catalytic tests (**Figure 4a** and **b**, Supporting Information, **Figure S7**). Over the EuOCl/TiO$_2$-a samples no europium-based phases were identified, indicating its high dispersion. On the other hand, reflections of Eu$_2$O$_3$ phase could be distinguished in the equilibrated EuOCl/SiC sample, suggesting (*i*) the lower europium dispersion upon reaction, and (*ii*) likely strong active phase-support electronic interactions that inhibits the transformation of Eu$_2$O$_3$ into EuOCl over SiC. Transmission electron microscopy (TEM) in high-angle annular dark field mode (HAADF) and high resolution TEM corroborated

the high and low europium dispersion in the EuOCl/TiO$_2$-a and

Figure 4. X-ray diffractograms and total surface area of a) EuOCl/TiO$_2$-a and b) EuOCl/SiC prior to (fresh) and after EOC and POC. The insets magnify the diffractograms in the region of 20°-40° 2θ. Marked reflections according to the JCPDS reference patterns: TiO$_2$-anatase (triangle), SiC (star), Eu$_2$O$_3$ (diamond). c) Transmission electron microscopy (TEM) in high-angle annular dark field mode (HAADF), and high resolution TEM of used EuOCl/TiO$_2$-a, and d) HAADF-TEM of used EuOCl/SiC. e) Ethylene space time yield (STY(C$_2$H$_4$); solid bars) and ethylene selectivity (open bars) in EOC at increasing reactants concentration (gray), and total pressure (orange), and in the presence of water (blue). The numbers in the sample code denote the molar feed ratio (C$_2$H$_6$:HCl:H$_2$O:O$_2$). f) Alkane conversion, product selectivity and ethylene space time yield *versus* time-on-stream over EuOCl/TiO$_2$-a extrudates in the oxychlorination of ethane at concentrated feeds and in the presence of water (C$_2$H$_6$:HCl:H$_2$O:O$_2$=12:12:12:6).

EuOCl/SiC catalysts, respectively (**Figure 4c** and **d**, Supporting Information, **Figure S8**).

Further evidence on the importance of the carrier selection comes from the alkane oxidation, and the alkyl chloride dehydrochlorination (in the presence or absence of oxygen) tests conducted over these catalysts (Supporting Information, **Figure S9** and **10**). It was rationalized that EuOCl/TiO$_2$-a possesses low tendency towards alkane combustion, and high activity in the dehydrochlorination of C$_2$H$_5$Cl, making it a very effective catalyst for ethylene production. On the other hand, it fails in POC due to its high reactivity in combusting C$_3$H$_7$Cl. EuOCl/SiC, instead, is more inert towards C$_3$H$_7$Cl oxidation. This together with its low tendency to combust the alkane, and its good activity in C$_3$H$_7$Cl makes it a much better catalyst for POC.

To further demonstrate the practical relevance of the presented catalytic technology, the best ethylene producer, EuOCl/TiO$_2$-a extrudates, was taken as representative, analyzed in greater details and evaluated its performance under more demanding conditions. Microscopy measurements by scanning TEM-HAADF with elemental mapping by energy-dispersive X-ray (EDX) showed the regularity of the surface as well as uniform distribution of europium along the extrudate before and after reaction (Supporting Information, **Figure S11**). Mercury porosimetry showed the preservation of the meso- and macroporosity of the extrudate (Supporting Information, **Figure S12a**). X-ray photoelectron spectroscopy of the samples evidenced the presence of Eu^{2+} on the catalytic surface, which slightly increases after being exposed to the reaction environment (Supporting Information, **Figure S12b**), suggesting the Eu^{3+}/Eu^{2+} to be the active redox couple, in line with other studies on Eu-based catalysis.[7b]

To verify the robustness of shaped EuOCl/TiO$_2$-a, we have studied the effect of higher reactants partial pressure and total pressure over this catalyst in EOC. A three-fold increase in the concentration of reactants led to a more than three times higher ethylene space time yield at ≥90% selectivity. Likewise, upon increasing the total pressure from atmospheric until 1.75 bar, a two-fold increment of STY(C$_2$H$_4$) was achieved at >90% selectivity (**Figure 4e**). Carbon elemental analysis (Supporting Information, **Table S3**) of the sample recovered after 5 h exposure to three times higher reactant concentration demonstrated the absence of coke. Moreover, we have tested EuOCl/TiO$_2$-a by using N$_2$ as the carrier gas instead of He and observed that the catalytic performance was preserved.

Although today mature technologies for HCl/H$_2$O separation are applied in industry,[11a,b] effective and tailored methods would be required to separate water since it is a net reaction product. In this view, we have studied the effect of stoichiometric water addition to EOC feed over EuOCl/TiO$_2$-a. Ethylene selectivity of ≥90% was attained despite a small drop in productivity, which could be partially restored by doubling all reactants partial pressures (**Figure 4e**), demonstrating that an operation with dry HCl is not critical to maintain the outstanding performance. Finally, we have evaluated EuOCl/TiO$_2$-a extrudates in a long-term test at higher reactants partial pressure and by water co-feeding, which showed its ability to retain the outstanding performance for over 150 h and its

mechanical, surface and bulk physicochemical properties (**Figure 4f**; Supporting Information, **Figure S12**). These promising results open the doors for further process-oriented studies targeting large-scale implementation, such as heat management, products separation (*i.e.* H_2O, HCl, CO_x), reactor design *etc.*, although relevant solutions can be extrapolated from applied technologies.[11]

In conclusion, we have discovered EuOCl as a highly promising catalytic technology for the selective one-step conversion of ethane and propane into olefins *via* oxychlorination chemistry, providing the highest single-pass yields of ethylene and propylene (90% and 40%, respectively) among any existing technology of olefin production. The performance of EuOCl was rationalized by (*i*) its balanced redox properties that allows to functionalize the alkane and to avoid combustion, and by (*ii*) its unpaired ability to dehydrochlorinate the formed alkyl chloride to olefin, enabling the recycling of the halogen source. Moreover, EuOCl is able to selectively process also mixtures of methane, ethane, and propane to produce ethylene and propylene, thereby strongly reducing separation costs of the alkanes in natural gas. Finally, we demonstrated the scalability of the EuOCl-based catalyst in extrudate form using widely available carriers. Titanium dioxide was identified as the best support for ethylene production, which maintained the outstanding performance for over 150 h on stream at both increased reactants partial pressure and by co-feeding water. These results show the practical relevance of the EuOCl-based chemistry for natural gas upgrading, and drives future research on several macroscopic engineering aspects for further demonstration of the applicability of this catalytic technology.

Experimental Section

Details on the catalyst preparation, characterization, and evaluation are provided as Supporting Information.

Acknowledgements

[1]   a) R. Lin, A. P. Amrute, J. Pérez-Ramírez, *Chem. Rev.* **2017**, *117*, 4182-4247; b) J. J. H. B. Sattler, J. Ruiz-Martinez, E. Santillan-Jimenez, B. M. Weckhuysen, *Chem. Rev.* **2014**, *114*, 10613-10653.

[2]   a) F. Cavani, N. Ballarini, A. Cericola, *Catal. Today* **2007**, *127*, 113-131; b) T. Ren, M. Patel, K. Blok, *Energy* **2006**, *31*, 425-451; c) F. J. Brazdil, *Top. Catal.* **2006**, *38*, 289-294.

[3]   E. McFarland, *Science* **2012**, *338*, 340-342.

[4]   a) C. A. Gärtner, A. C. van Veen, J. A. Lercher, *ChemCatChem* **2013**, *5*, 3196-3217; b) D. A. Goetsch, L. D. Schmidt, *Science* **1996**, *271*, 1560-1562; c) A. S. Bodke, D. A. Olschki, L. D. Schmidt, E. Ranzi, *Science* **1999**, *285*, 712-715; d) R. Horn, R. Schlögl, *Catal. Lett.* **2015**, *145*, 23-39.

[5]   a) V. Paunović, G. Zichittella, R. Verel, A. P. Amrute, J. Pérez-Ramírez, *Angew. Chem. Int. Ed.* **2016**, *55*, 15619-15623; *Angew. Chem.* **2016**, *128*, 15848-15852; b) G. Zichittella, V. Paunović, A. P. Amrute, J. Pérez-Ramírez, *ACS Catal.* **2017**, *7*, 1805-1817.

[6]   a) L. Xueju, L. Jie, Z. Guangdong, Z. Kaiji, L. Wenxing, C. Tiexin, *Catal. Lett.* **2005**, *100*, 153-159; b) J. P. Henley, M. E. Jones, D. A. Hickman, K. A. Marshall, D. J. Reed, W. D. Clarke, M. M. Olken, L. E. Walko (Dow Global Technologies Inc.), US-B1 6933417, **2005**; c) R. T. Carrol, E. J. De Witt, C. Falls, L. E. Trapasso (B. F. Goodrich Company), US 3173962, **1965**; d) A. Shalygin, E. Paukshtis, E. Kovalyov, B. Bal'zhinimaev, *Front. Chem. Sci. Eng.* **2013**, *7*, 279-288; e) C. Li, G. Zhou, L. Wang, S. Dong, J. Li, T. Cheng, *Appl. Catal., A* **2011**, *400*, 104-110; f) D. Shi, R. Hu, Q. Zhou, L. Yang, *Chem. Eng. J.* **2016**, *288*, 588-595; g) A. E. Schweizer, M. E. Jones, D. A. Hickman (Dow Global Technologies Inc.), US-B2 6984763, **2006**.

[7]   a) N. Rahimi, R. Karimzadeh, *J. Catal.* **2016**, *344*, 524-534; b) V. Paunović, R. Lin, M. Scharfe, A. P. Amrute, S. Mitchell, R. Hauert, J. Pérez-Ramírez, *Angew. Chem. Int. Ed.* **2017**, doi:10.1002/anie.201704406; *Angew. Chem.* **2017**, doi:10.1002/ange.201704406.

[8]   a) N. Rahimi, R. Karimzadeh, *Appl. Catal., A* **2011**, *398*, 1-17; b) H. Zimmermann, R. Walzl, *Ullmann's Encyclopedia of Industrial Chemistry*, *Vol. 13*, Wiley-VCH, Weinheim, **2012**, pp. 465-529.

[9]   B. G. Hashiguchi, M. M. Konnick, S. M. Bischof, S. J. Gustafson, D. Devarajan, N. Gunsalus, D. H. Ess, R. A. Periana, *Science* **2014**, *343*, 1232-1237.

[10]   a) E. N. Givens, C. J. Plank, E. J. Rosinki (Mobil Oil Corporation), US-A 3960978, **1974**; b) A. Giusti, S. Gusi, G. Bellussi, V. Fattore (Eniricerche S. P. A.), US-A 4831201, **1989**.

[11]   a) J. A. Cowfer, M. B. Gorensek, *Kirk-Othmer Encyclopedia of Chemical Technology*, Wiley-VCH, Weinheim, **2006**; b) Sulzer-ChemTech Separation Technology for the Hydrocarbon Processing Industry, www.sulzer.com, accessed May 20th, **2017**, 10:00 GMT; c) Honeywll-UOP Technology for Purification of Olefin and Polymer Process Streams, www.uop.com, accessed May 20th, **2017**, 11:00 GMT.

Entry for the Table of Contents

COMMUNICATION

Bifunctionality is the key: Ethylene and propylene, can be generated from ethane, propane, or mixtures of methane, ethane and propane over europium oxychloride *via* oxychlorination chemistry at yields surpassing any existing technology for olefin production. Its performance can be preserved in technical form, testifying the practical relevance of this catalytic technology for olefin production.
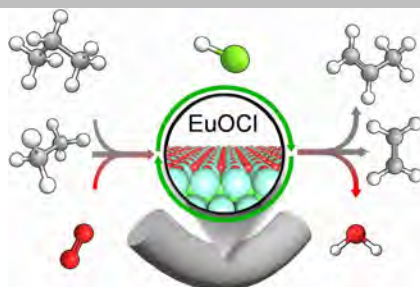
Guido Zichittella, Nicolas Aellen, Vladimir Paunović, Amol P. Amrute, and Javier Pérez-Ramírez*

Supporting Information

Olefins from Natural Gas via Oxychlorination Catalysis

Guido Zichittella, Nicolas Aellen, Vladimir Paunović, Amol P. Amrute, and Javier Pérez-Ramírez*

* Corresponding author. E-mail: jpr@chem.ethz.ch

Catalyst preparation

Commercial CeO_2 (Sigma-Aldrich, nanopowder, 99.9%) and TiO_2 (Sigma-Aldrich, rutile nanopowder, 99.5%) were calcined in static air at 1173 and 873 K, respectively, prior to their use in the catalytic tests. $(VO)_2P_2O_7$ was prepared by refluxing a suspension of V_2O_5 (15.0 g, Sigma Aldrich, 99.5%) in isobutanol (90 cm^3, Acros Organics, 99%) and benzyl alcohol (60 cm^3, Sigma-Aldrich, 99%) for 3 h. After cooling down to room temperature, H_3PO_4 (Sigma-Aldrich, 85%) was added to attain a molar P:V ratio of 1.2, and the mixture was then refluxed for another 16 h. The resulting solid was recovered by filtration, washed with isobutanol and methanol (Fluka, 99.9%), dried in vacuum (50 mbar) at 373 K for 12 h, and thermally activated in flowing N_2 at 873 K. $FePO_4$ was synthesized by mixing an aqueous solution of $Fe(NO_3)_3·9H_2O$ (Sigma-Aldrich, 99%) and $NH_4H_2PO_4$ (Acros Organics, 99%) in a molar P:Fe ratio of 1 for 2 h, followed by drying in vacuum (50 mbar) at 373 K for 12 h and calcination in flowing air at 873 K. For the preparation of EuOCl, first Eu_2O_3 precursor was obtained by dissolving $Eu(NO_3)_3·6H_2O$ (ABCR, 99.9%) in deionized water and H_2O_2 (Acros Organics, 35 wt.%) was added to the solution to attain a molar H_2O_2:Eu ratio of 3. The obtained solution was precipitated by dropwise addition of aqueous NH_4OH (Sigma-Aldrich, 25%) until a pH of 10.5 was reached. The slurry was stirred for 4 h and washed with deionized water. The precipitate was separated by filtration, dried at 373 K for 12 h, and calcined in static air at 873 K. In the second step, Eu_2O_3 (4.0 g) was transformed into EuOCl by treatment in the oxychlorination feed mixture (molar ratio C_2H_6:HCl:O_2:Ar:He = 30:30:15:22.7:2.5, total flow rate $F_T = 25$ cm^3 min^{-1}) at 773 K for 4 h. Supported Eu-based catalysts denoted as EuOCl/SiC, EuOCl/SiO_2, EuOCl/ZrO_2, and EuOCl/TiO_2-a were prepared by impregnating an aqueous solution of $Eu(NO_3)_3·6H_2O$ on pre-calcined (static air, 873 K) carriers in extrudate form (diameter: 3.2 mm, length: 3-5 mm) comprising β-SiC (SICAT, 99%), SiO_2 (Saint-Gobain NORPRO, 99%), ZrO_2- monoclinic (Alfa Aesar, 99%), and TiO_2-anatase (Alfa Aesar, 99%) extrudates, respectively. An appropriate amount of $Eu(NO_3)_3·6H_2O$, targeting an europium content of 10 wt.% in the final catalyst, was dissolved in a volume of deionized water equivalent to the pore volume of the support as determined from N_2 sorption, and the obtained solution was added dropwise to the carrier under continuous mixing. The impregnated extrudates were dried at 333 K for 12 h, and calcined in static air at 873 K. Prior to catalytic evaluation, the technical catalysts were activated by treatment in a feed mixture containing HCl:O_2:Ar:He = 10:10:4.5:75.5 at 773 K for 2 h. All thermal treatments were performed using a heating rate of 5 K min^{-1} and a holding time of 5 h.

Catalyst characterization

X-ray diffraction (XRD) patterns were acquired in a PANalytical X'Pert PRO-MPD diffractometer and Cu-Kα radiation ($\lambda = 0.154$ nm). The data was recorded in the 10-70° 2θ range with an angular step size of 0.017° and a counting time of 0.26 s per step. N_2 sorption at 77 K was measured in a Micromeritics TriStar analyzer. Prior to the measurements, the samples were outgassed to 50 mbar at 573 K for 12 h. The Brunauer-Emmett-Teller (BET) method was applied to calculate the total surface area, S_{BET}, in m^2 g^{-1}. To characterize the internal organisation of the shaped catalysts, individual extrudates were embedded into a Bakelite resin at 453 K, then sanded to the desired position by using SiC abrasive papers in decreasing grain size order (46 μm, 30 μm, 15 μm), and finally polished to the desired position with a

diamond paste in a decreasing size order (6 μm, 3 μm, 1 μm, 0.25 μm). After each polishing step, the sample was ultrasonicated in ethanol and then dried to ensure complete removal of the abrasive paste. Prior to the microscopy measurements, the sample was coated with carbon (2 nm) to minimize charging. HAADF-STEM (high-angle annular dark field scanning transmission electron microscopy) imaging and EDX (energy dispersive X-ray) mapping of the resulting extrudate cross-sections was conducted using a FEI Quanta 200 F microscope operated at 20 kV. Transmission electron microscopy (TEM) in HAADF mode and high-resolution TEM (HRTEM) measurements were performed using a FEI Tecnai F30 ST microscope (field emission gun, operated at 300 kV). Mercury porosimetry was measured in a Micromeritics AutoPore IV 9520 operated from vacuum to 418 MPa. Samples were degassed *in situ* prior to measurement. A contact angle of 140° for mercury and a pressure equilibration of 10 s were applied. The carbon content in the catalysts was determined by a LECO TruSpec Micro elemental analyzer. X-ray photoelectron spectroscopy (XPS) measurements were performed on a Physical Electronics Quantum 2000 X-ray photoelectron spectrometer using monochromatic Al-Kα radiation, generated from an electron beam operated at 15 kV, and equipped with a hemispherical capacitor electron-energy analyzer. The solids were analyzed at the electron take-off angle of 45° and the pass energy of 46.95 eV. A compensation for sample charging was obtained by referencing all the spectra to the C 1s at 284.5 eV.

Catalyst testing

The catalytic tests were performed at ambient pressure in a continuous-flow fixed-bed reactor set-up (**Scheme S1**). The quartz tubular reactor of 10 mm or 15 mm internal diameter was loaded with 1.0 g of catalyst particles (d_p = 0.4-0.6 mm) or extrudates (diameter: 3.2 mm, length: 3-5 mm), respectively, sitting on a plug of quartz wool, and placed in an electrical oven equipped with a K-type thermocouple inserted in a coaxial quartz thermowell whose tip reaches the center of the catalyst bed. Prior to the tests, the catalyst was heated in a He flow till the desired bed temperature (T = 473-873 K), and then stabilized for 30 min under these conditions before the reaction mixture was admitted. The gases CH_4 (PanGas, purity 5.5), C_2H_6 (PanGas, purity 3.5), C_3H_8 (PanGas, purity 3.5), HCl (Air Liquide, purity 2.8, anhydrous), O_2 (PanGas, purity 5.0), C_2H_5Cl (PanGas, 5 mol.% in He 5.0), Ar (PanGas, purity 5.0) (internal standard), N_2 (PanGas, purity 5.0) (carrier gas), and He (PanGas, purity 5.0) (carrier gas) were fed by digital mass flow controllers (Bronkhorst®) to achieve a desired feed composition at a total volumetric flow, F_T, of 6 L STP h^{-1} (space velocity, F_T/W_{cat} = 6 L STP h^{-1} g^{-1}). 1-C_3H_7Cl (Fluka, 97%) or deionized water were vaporized in the carrier gas stream using a syringe pump (Nexus 6000, Chemyx) and a vaporizer operated at 343 K, accommodating a quartz T-connector filled with glass beads. Reactions and feed compositions studied in this work are summarized in **Table S1**. The downstream lines were heat traced at 393 K in order to prevent condensation of the reactants and products. The effluent gas stream was neutralized by passing it through an impinging bottle containing an aqueous 1 M NaOH solution. The content of the carbon-containing compounds (methane, ethane, ethylene, propane, propylene, their chlorinated derivatives, CO, and CO_2) in the reactor-outlet gas stream was determined with a gas chromatograph equipped with a GS-CarbonPLOT column (113-3133) coupled to a mass spectrometer (GC-MS, Agilent GC 6890, MS 5973N). Cl_2 was quantified by off-line iodometric titration (using a Mettler Toledo G20 Compact Titrator) of triiodide, formed by purging a stream containing the

molecular chlorine through an aqueous 0.1 M KI solution, with 0.01 M sodium thiosulfate solution (Sigma-Aldrich, 99.99%). The content of HCl was determined from the same KI solution by an acid-base titration with aqueous 0.01 M NaOH solution (Sigma-Aldrich, 99.99%), after neutralizing the formed triiodide with sodium thiosulfate.

The conversion of reactant i, $X(i)$, (i: CH_4, C_2H_6, C_3H_8, C_2H_5Cl, C_3H_7Cl, and HCl) was calculated using Eq. 1,

$$X(i) = \frac{n(i)^{inlet} - n(i)^{outlet}}{n(i)^{inlet}} \cdot 100, \%$$

Eq. 1

where $n(i)^{inlet}$ and $n(i)^{outlet}$ are the molar flows of the reactant i at the inlet and outlet of the reactor, respectively. The conversion of HCl, $X(HCl)$, was calculated using Eq. 2,

$$X(HCl) = \frac{2 \cdot n(Cl_2)^{outlet}}{n(HCl)^{inlet}} \cdot 100, \%$$

Eq. 2

where $n(HCl)^{inlet}$ and $n(Cl_2)^{outlet}$ denote the molar flows of HCl and Cl_2 at the reactor inlet and outlet, respectively. Selectivity, $S(j)$, and yield, $Y(j)$, of product j (j: CH_3Cl, C_2H_4, C_3H_6, C_2H_5Cl, C_2H_3Cl, Cl_2, CO, and CO_2) were determined according to Eqs. 3 and 4,

$$S(j) = \frac{n(j)^{outlet} \cdot N_C(j)}{\sum n(j)^{outlet} \cdot N_C(j)} \cdot 100, \%$$

Eq. 3

$$Y(j) = \frac{X(i) \cdot S(j)}{100}, \%$$

Eq. 4

where $n(j)^{outlet}$ is the molar flow of the product j at the reactor outlet, $N_C(j)$ is the number of carbon atoms in the compound j.

The error of the carbon, ε_C, and chlorine balance, ε_{Cl}, was determined using Eqs. 5 and 6,

$$\varepsilon_C = \frac{n(i)^{inlet} \cdot N_C(i) - \left(n(i)^{outlet} \cdot N_C(i) + \sum n(j)^{outlet} \cdot N_C(j)\right)}{n(i)^{inlet} \cdot N_C(i)} \cdot 100, \%$$

Eq. 5

$$\varepsilon_{Cl} = \frac{\sum n(i)^{inlet} \cdot N_{Cl}(i) - \left(\sum n(j)^{outlet} \cdot N_{Cl}(j) + \sum n(i)^{outlet} \cdot N_{Cl}(i)\right)}{\sum n(i)^{inlet} \cdot N_{Cl}(i)} \cdot 100, \%$$

Eq. 6

where $n(i)^{inlet}$ denotes the molar flow of the reactant i at the reactor inlet, $n(i)^{oulet}$ and $n(j)^{outlet}$ are the molar flows of the reactant i and product j (in addition to the alkyl chlorides, j also denotes the molecular halogen Cl_2 in Eq. 6) at the reactor outlet, respectively. $N_C(i)$ and $N_C(j)$ are the numbers of carbon atoms in the reactant i and j, respectively, while $N_{Cl}(i)$ and $N_{Cl}(j)$ refer to the numbers of chlorine atom in the compounds i and j, respectively. The carbon and chlorine mass balance in all the catalytic tests were closed at 95% or higher. Each measurement was stabilized for at least 1 h at every investigated condition to reach steady-state. All catalytic data points were determined as an average of at least two measurements. After the tests, the catalyst bed was quenched to room temperature in He flow and the catalyst was collected for an *ex situ* characterization.

Table S1. Reactions and feed compositions studied in this work.

Reaction	Concentration / vol.%									
	C_2H_6	C_3H_8	CH_4	HCl	H_2O	C_2H_5Cl	C_3H_7Cl	O_2	Ar[a]	He[b]
Oxychlorination of										
- Ethane	1.5-18	-	-	0-18	6-12	-	-	3-9	4.5	85-50.5[c]
- Propane	-	1.5-6	-	0-15	-	-	-	3-9	4.5	85-71.5
- Methane	-	-	6	6	-	-	-	3	4.5	80.5
- Alkane mixtures	1.5-3	1	3.5-8.5	6-15	-	-	-	3-10	4.5	80.5-65.5
Dehydrochlorination of										
- Ethyl chloride	-	-	-	-	-	1	-	-	4.5	94.5
- Propyl chloride	-	-	-	-	-	-	1	0.5	4.5	94.5-94
Oxidation of HCl	-	-	-	6	-	-	-	3	4.5	86.5

[a] internal standard.
[b] carrier gas.
[c] N_2 was used as the carrier gas.

Table S2. Temperatures and feed concentrations of HCl, O_2, and alkane studied in the oxychlorination of ethane and propane over EuOCl as reported in **Figures 2c** and **d** of the main article.

Temperature	
■	623 K
●	680 K
▲	723 K
▼	773 K
◆	810 K
⬟	847 K

Concentration of HCl	
■	0 vol.%
●	1 vol.%
▲	3 vol.%
▼	6 vol.%
◆	15 vol.%

Concentration of O_2	
■	3 vol.%
●	6 vol.%

Concentration of alkane	
■	6 vol.%
●	3 vol.%
▲	1.5 vol.%

Table S3. Alkane-based gas-hourly-space-velocity (GHSV) investigated in the oxychlorination of ethane and propane over bulk and supported catalysts, as reported in **Figures 2a** and **b** of the main article and **Figures S1** and **S6**.

Catalyst	GHSV/ h^{-1}
CeO_2	415
$(VO)_2P_2O_7$	155
TiO_2	240
$FePO_4$	215
EuOCl	380
EuOCl/SiC	165
EuOCl/SiO_2	100
EuOCl/ZrO_2	295
EuOCl/TiO_2	245

Table S4. Carbon content of the fresh and used europium oxychloride-based catalysts.

Catalyst	Reaction	Alkane:HCl:O$_2$/ vol.%	Temperature / K	Reaction time / h	C content / wt.%
EuOCl	fresh	-	-	-	0.10
EuOCl	EOC	6:6:3	823	110	0.06
EuOCl	POC	6:6:3	723	5	0.04
EuOCl/TiO$_2$	fresh	-	-	-	0.07
EuOCl/TiO$_2$	EOC	6:6:3	723-813	5	0.05
EuOCl/TiO$_2$	EOC	18:18:9	773	5	0.03
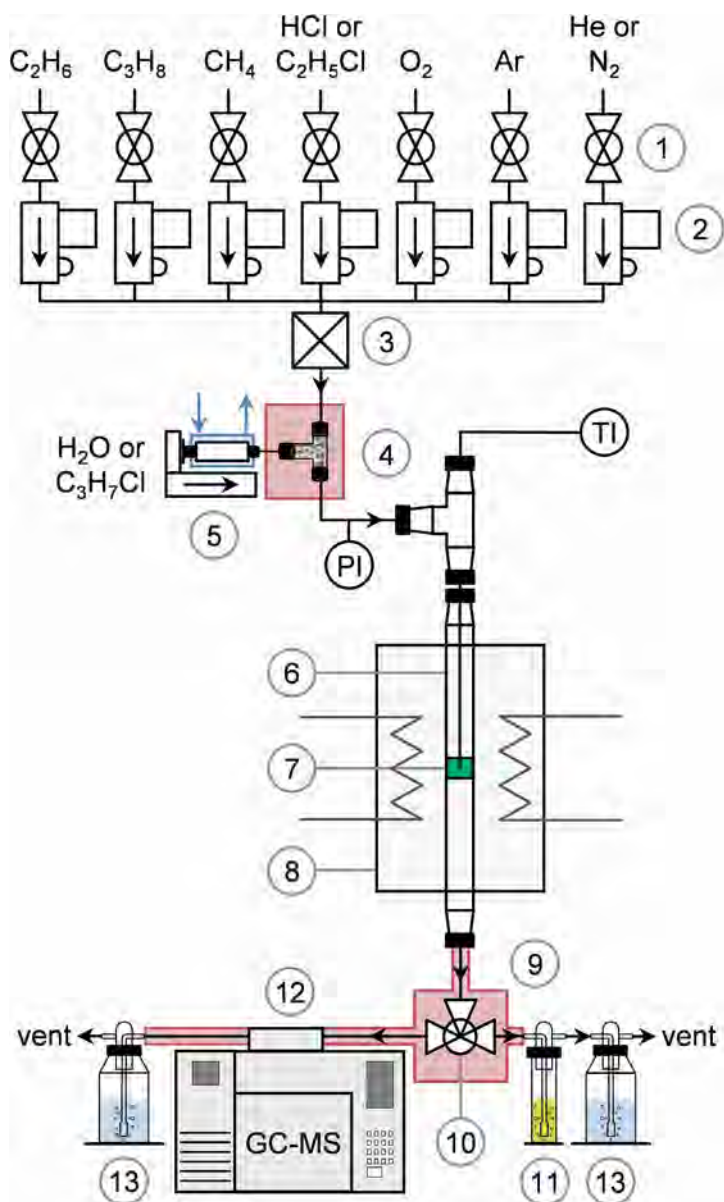
Scheme S1. Flowsheet of the laboratory set-up for the continuous-flow oxychlorination of light alkanes, oxidation of HCl or light alkanes, and alkyl chloride dehydrochlorination. 1: two-way on-off valves, 2: mass flow controllers, 3: mixer, 4: vaporizer, 5: syringe pump with water-cooling system, 6: quartz reactor, 7: catalyst bed, 8: oven, 9: heat tracing, 10: three-way sampling valve, 11: KI impinging bottle, 12: gas chromatograph-mass spectrometer (GC-MS), 13: NaOH scrubbers, PI: pressure indicator, and TI: temperature indicator.
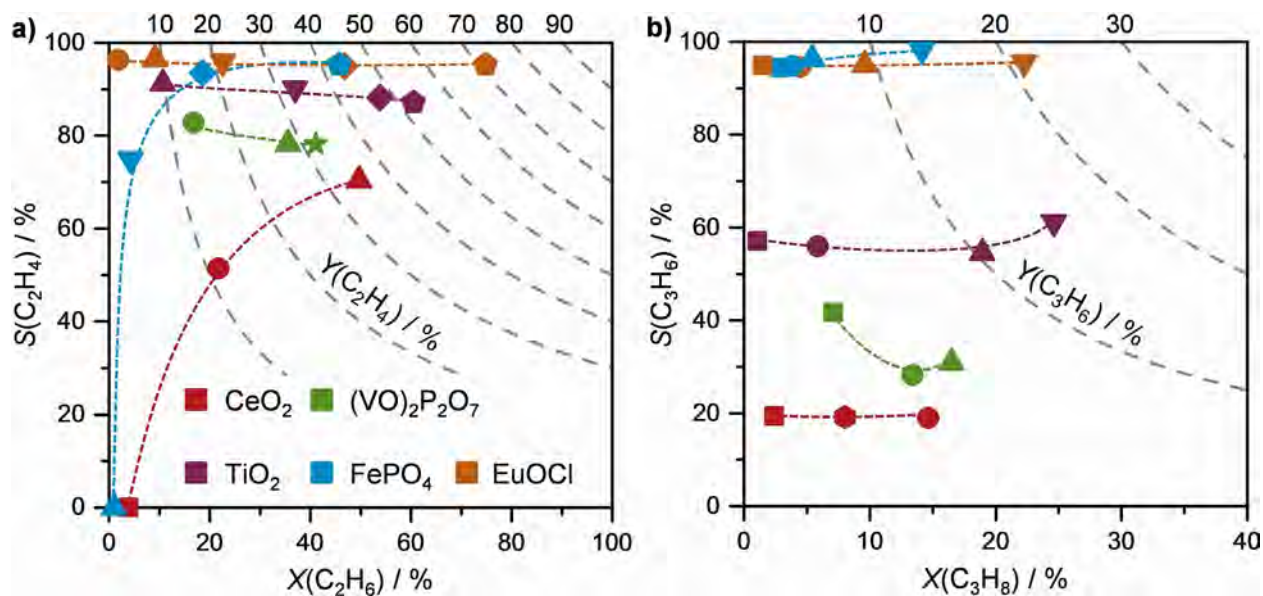
Figure S1. Olefin selectivity *versus* alkane conversion over the catalysts in the oxychlorination of **a)** ethane and **b)** propane. The alkane conversion was varied by tuning the reaction temperature (■ = 623 K, ⬣ = 650 K, ● = 680 K, ▲ = 723 K, ★ = 743 K, ▼ = 773 K, ◆ = 810 K, ⬟ = 847 K) at constant space velocity. Alkane-based GHSV = 155-415 h^{-1} (**Table S3**). The dotted gray lines denote the olefin yield, Y(olefin) = X(alkane) · S(olefin). The color codes for the catalysts as given in **a)** also apply to **b)**.
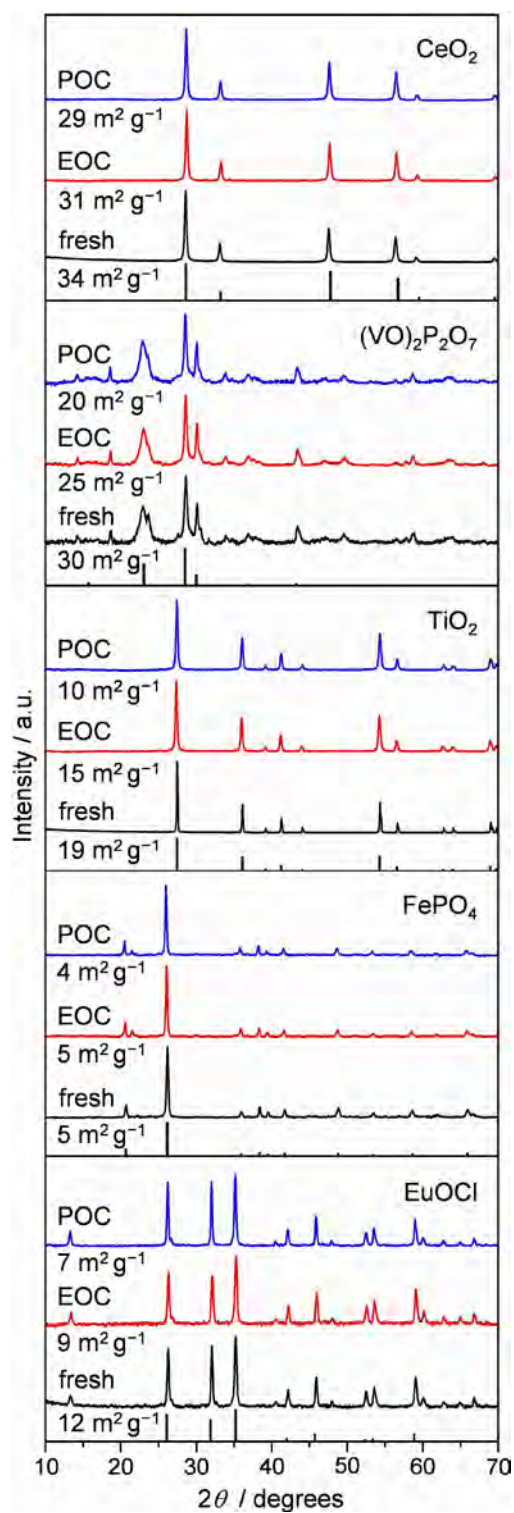
Figure S2. X-ray diffractograms and total surface area of the bulk catalysts prior to (fresh) and after the oxychlorination of ethane (EOC) and propane (POC). The diffraction lines below the diffractograms belong to CeO_2 (ICDD-PDF 04-0593), $(VO)_2P_2O_7$ (ICDD-PDF 50-0380), TiO_2-rutile (ICDD-PDF 83-242), $FePO_4$ (ICDD-PDF 71-3498), and EuOCl (ICDD-PDF 73-7281).
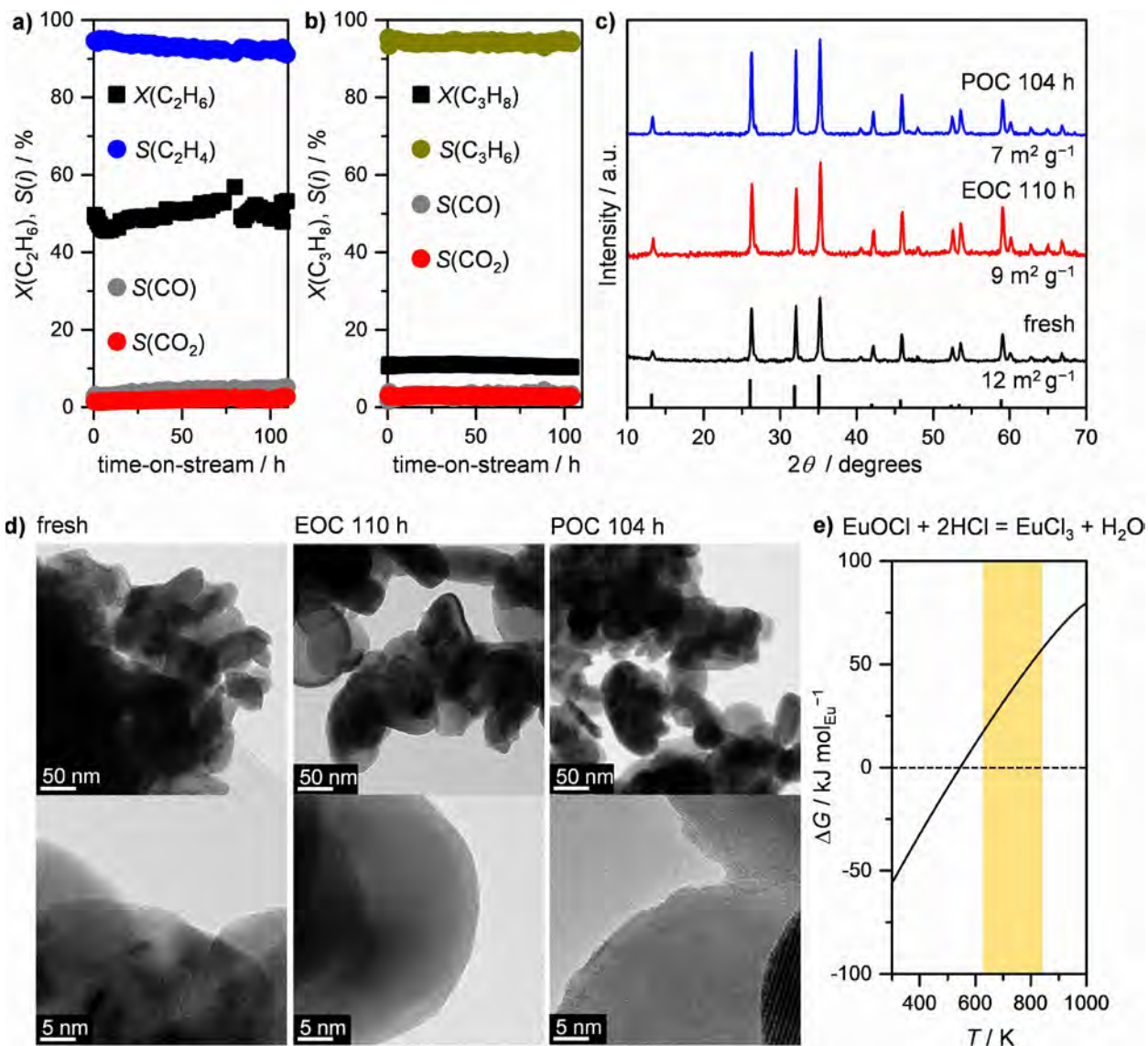
Figure S3. Alkane conversion and product selectivity *versus* time-on-stream over europium oxychloride in **a)** EOC at 823 K and **b)** POC at 723 K. **c)** X-ray diffractograms and total surface area of the EuOCl samples prior to (fresh) and after the reactions. The numbers in the sample code denote the total time of the corresponding catalytic run. The vertical lines below the diffractogram of the fresh sample correspond to EuOCl (ICDD-PDF 73-7281). **d)** High-resolution transmission electron micrographs of the samples. **e)** Gibbs free energy (ΔG) *versus* temperature for the transformation of EuOCl into EuCl$_3$. The yellow box denotes the operating window of the presented catalytic technology. The thermodynamic calculations were performed using a HSC Chemistry® V9 by Outotec.
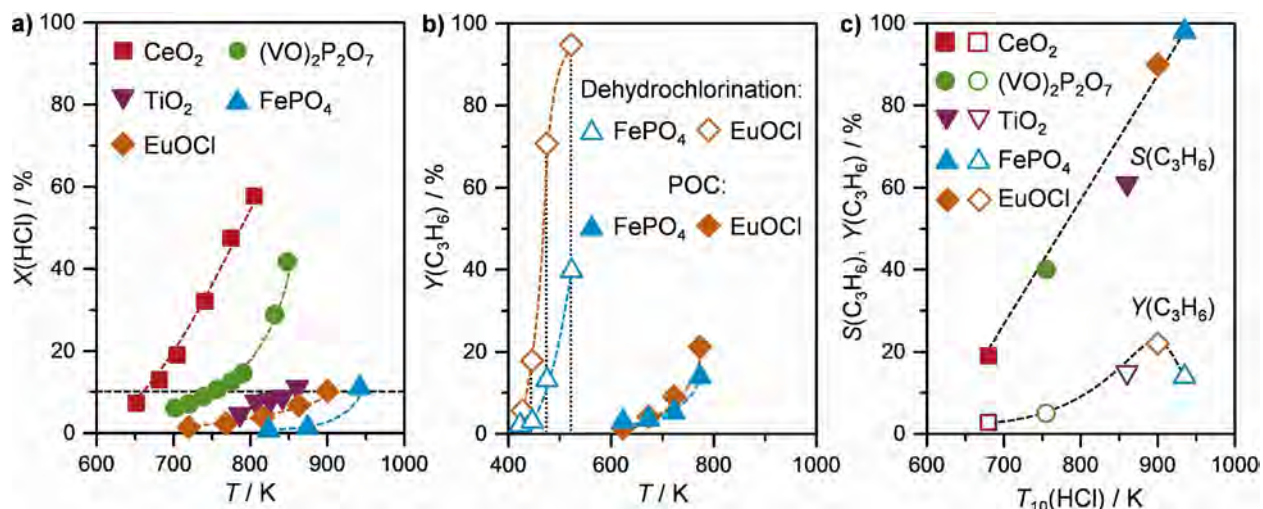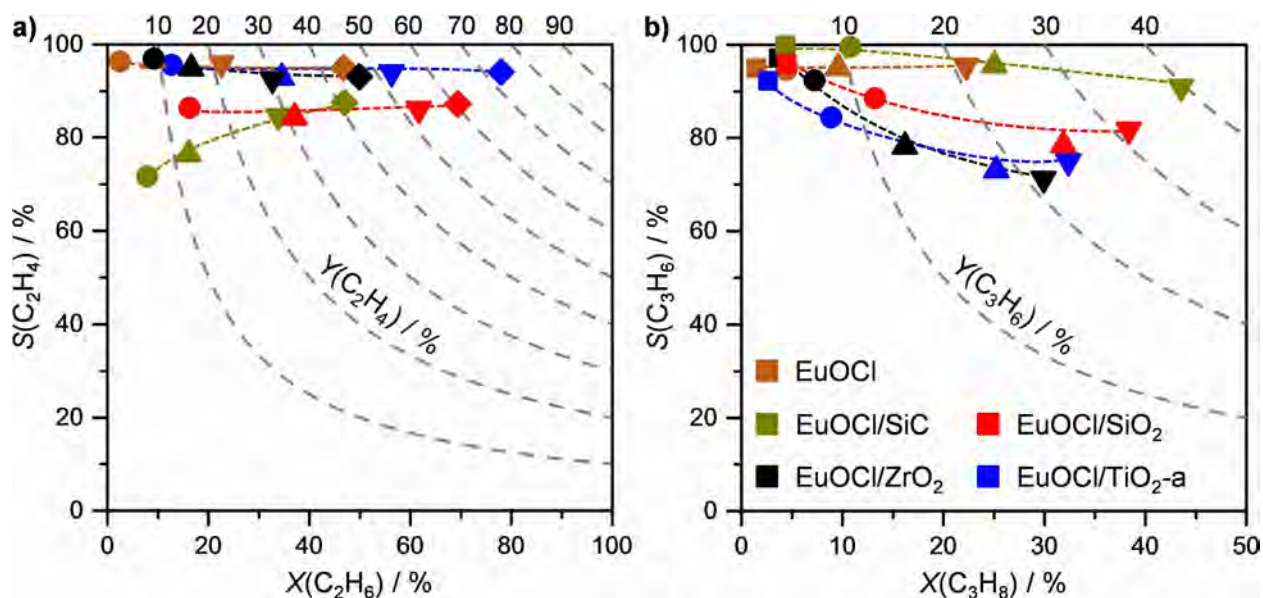
Figure S4. a) HCl conversion *versus* temperature in the oxidation of HCl to Cl$_2$ over the catalysts. The temperature at which 10% HCl conversion is achieved (T_{10}(HCl), dashed horizontal line) is taken as a relative measure of the oxidizing ability of the catalytic material under representative oxychlorination conditions. **b)** Yield of propylene *versus* temperature in the dehydrochlorination of C$_3$H$_7$Cl (open symbols) and in POC (solid symbols) over EuOCl and FePO$_4$. **c)** Selectivity (solid symbols) and yield (open symbols) of propylene in POC *versus* T_{10}(HCl) derived from **a)**.
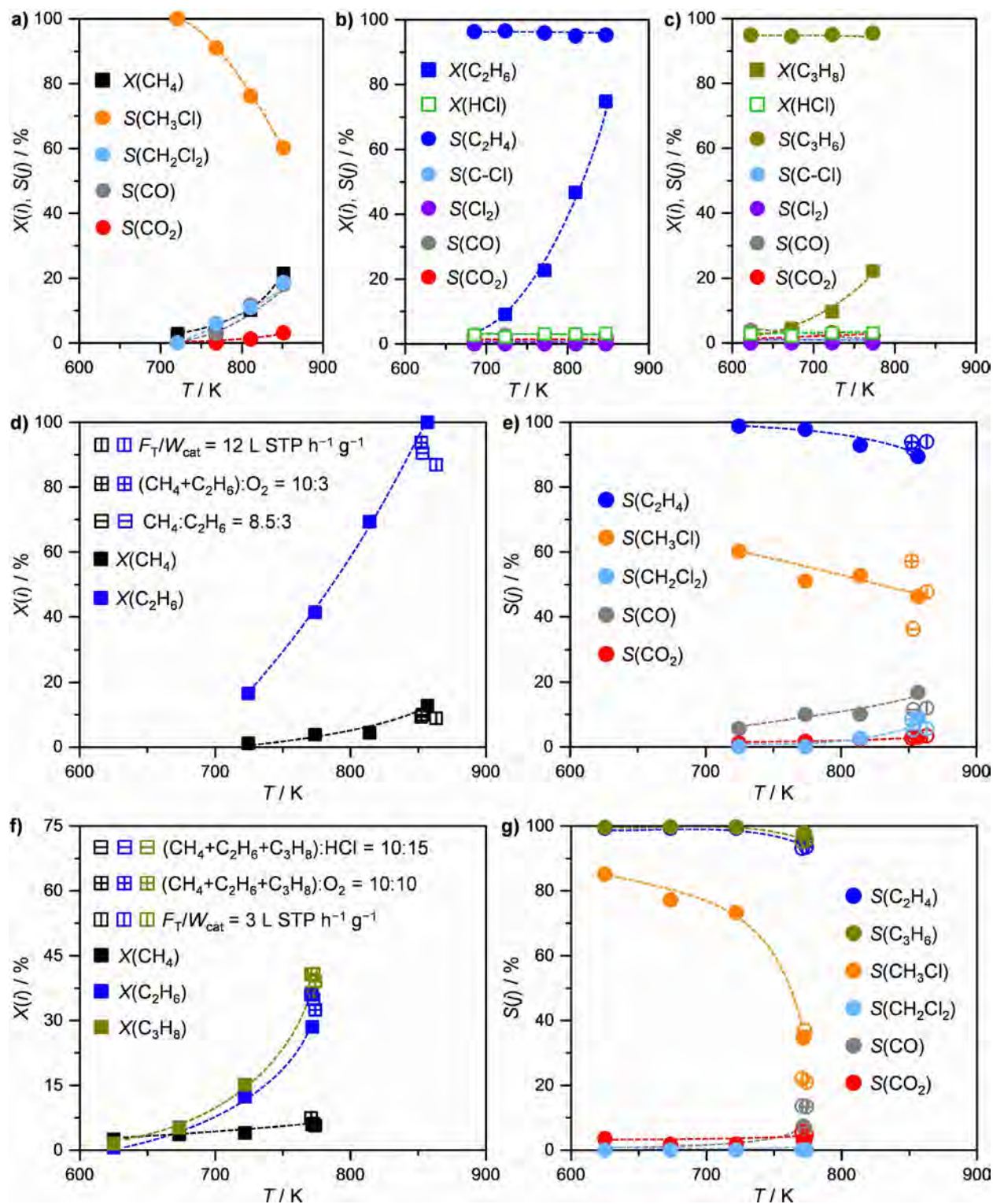
Figure S5. Conversion and selectivity *versus* temperature in the oxychlorination of **a)** methane, **b)** ethane (EOC), **c)** propane (POC), and **d)**, **f)**, and **g)** mixtures of the three alkanes (MEPOC) over EuOCl. S(C-Cl) in **b)** and **c)** refers to the combined selectivity to chlorinated hydrocarbons, namely C_2H_5Cl, $C_2H_4Cl_2$, and

C$_2$H$_3$Cl in EOC, and C$_3$H$_7$Cl and C$_3$H$_5$Cl in POC. The evaluation of the C-based selectivities in the tests of alkane mixtures can be challenging due to the simultaneous introduction of different carbon sources. Nevertheless, the evaluation of EuOCl in the oxychlorination experiments with the single alkanes verified the absence of both cracking and coupling reactions (**a)** to **c)**). Consequently, we have based the selectivity to ethylene and propylene on the amount of reacted ethane and propane, respectively, whereas the selectivity to CO and CO$_2$ were based on the total carbon converted. The alkane conversion and alkene selectivity obtained in the tests with pure alkanes and with the alkane mixtures are compared in **d)**. **e)** Alkane conversion (solid bar) and alkene selectivity (open bar) in EOC, POC, and MEPOC. The numbers in the reaction code in **e)** denote the feed HCl concentration in vol.% in the test. Reaction parameters, such as temperature, space velocity (F_T/W_{cat}), (CH$_4$+C$_2$H$_6$+C$_3$H$_8$):O$_2$ ratio, and (CH$_4$+C$_2$H$_6$+C$_3$H$_8$):HCl ratio, were varied (open symbols) in **f)** and **g)** in order to assess their impact on the catalytic performance. Standard conditions for the ternary alkane mixture in **f)** and **g)** (solid symbols): F_T/W_{cat} = 6 L STP h^{-1} g^{-1}; CH$_4$:C$_2$H$_6$:C$_3$H$_8$:HCl:O$_2$:Ar:He = 7.5:1.5:1:10:5:4.5:70.5.

Figure S6. Alkene selectivity *versus* alkane conversion over the bulk EuOCl and supported EuOCl (10 wt.% Eu) catalysts in the oxychlorination of **a)** ethane and **b)** propane. The alkane conversion was changed by varying the reaction temperature ($\blacksquare$ = 623 K, $\bullet$ = 680 K, $\blacktriangle$ = 723 K, $\blacktriangledown$ = 773 K, $\blacklozenge$ = 810 K) at constant space velocity. Conditions: alkane-based GHSV = 100-295 h^{-1} (**Table S3**). The dashed gray lines denote the yield of olefin, Y(olefin) = X(alkane)·S(olefin). The alkene selectivity at different alkane conversion levels are compared to those obtained over bulk EuOCl in both reactions. Based on this rationale, the catalysts can be classified into two different classes, which differ in EOC and POC. In the first reaction, the first class is represented by EuOCl/SiC and EuOCl/SiO$_2$, which could not reach ethylene selectivity above 87%. The second class is represented by EuOCl/ZrO$_2$ and EuOCl/TiO$_2$-a, which could preserve the ethylene selectivity of the bulk EuOCl. In addition to that, EuOCl/TiO$_2$-a showed even higher activity compared to the bulk catalyst, emerging as an outstanding technical catalyst for ethylene production. However, in POC EuOCl/SiC emerged as the best catalyst, achieving propylene selectivity of >90% over the whole temperature range investigated and even higher activity compared to bulk EuOCl, reaching 40% yield of propylene.
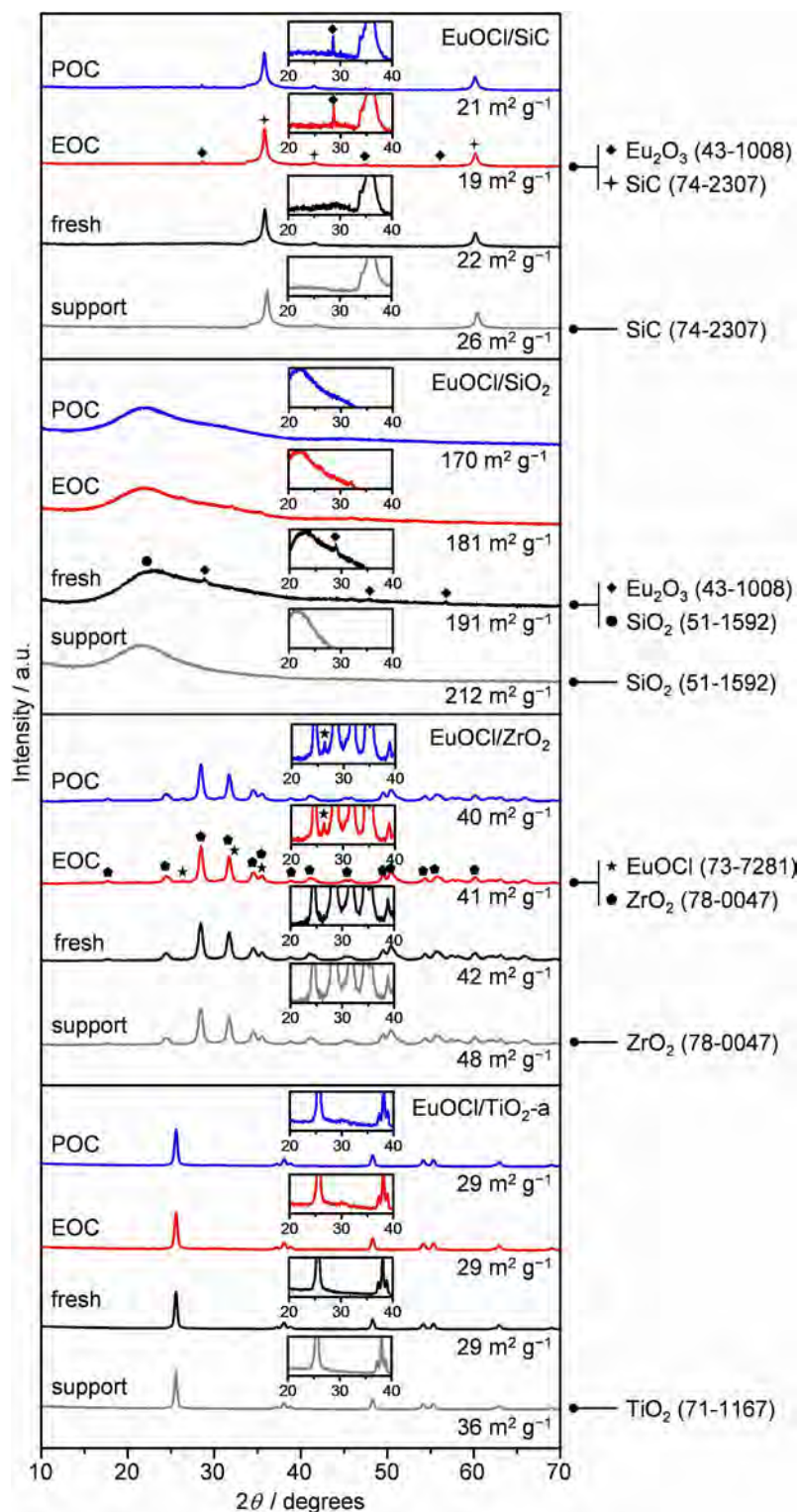
Figure S7. X-ray diffractograms and total surface area of the supports, and of the supported EuOCl catalysts (10 wt.% Eu) in extrudate form prior to (fresh) and after the oxychlorination of ethane (EOC) and propane (POC). The insets magnify the X-ray diffractograms in the region of 20°-40° 2θ, whereas the right panel provides the identified crystalline phases and ICDD-PDF numbers.
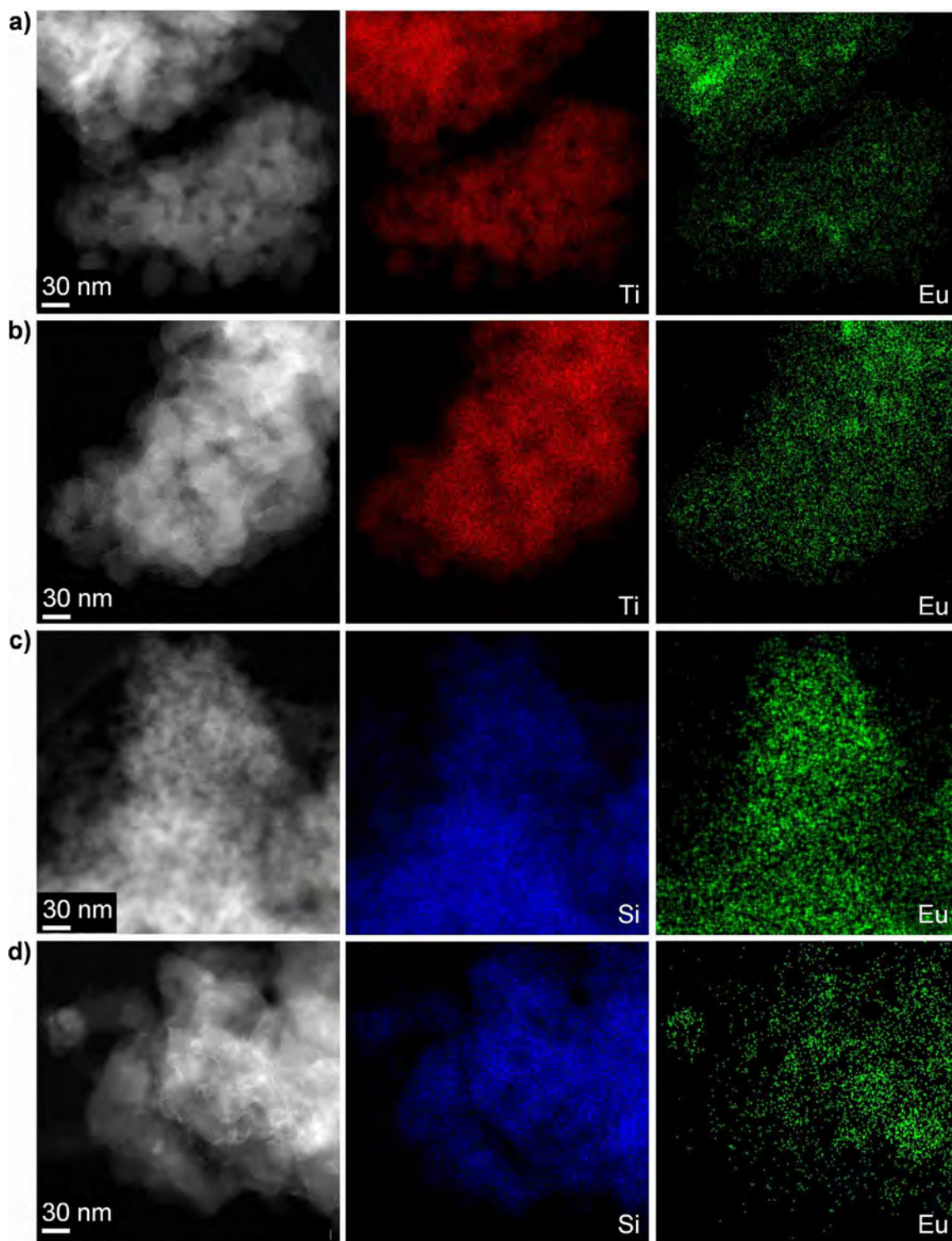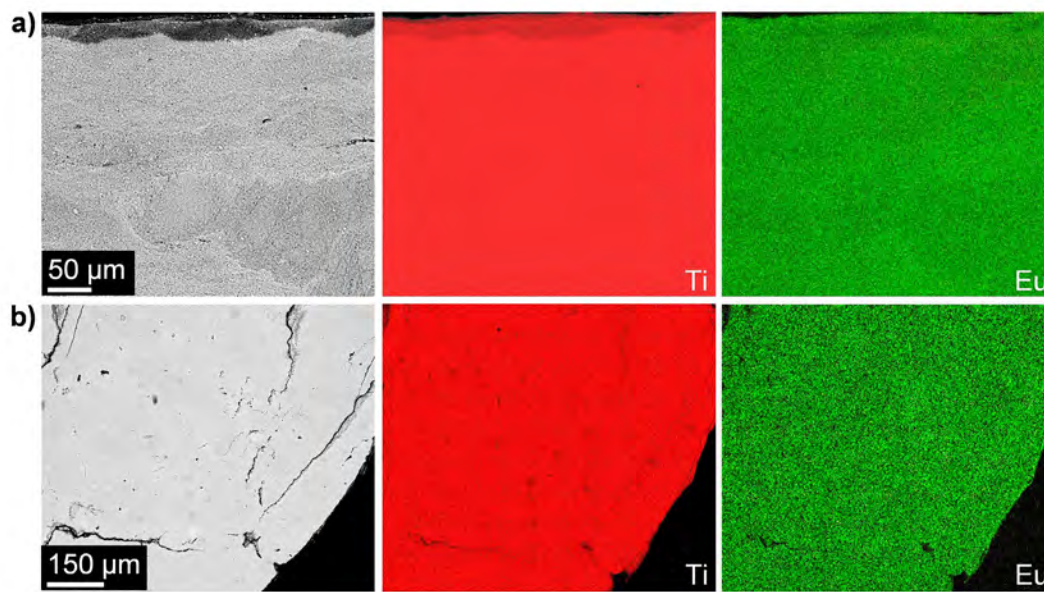
Figure S8. Transmission electron microscopy (TEM) in high-angle annular dark field mode (HAADF) with elemental mapping by means of energy-dispersive X-ray (EDX), and high resolution TEM of the fresh (top) and used (bottom) **a)**, **b)** EuOCl/TiO$_2$-a, and **c)**, **d)**, EuOCl/SiC samples. Elemental color code: Eu: green; Ti: red; Si: blue.
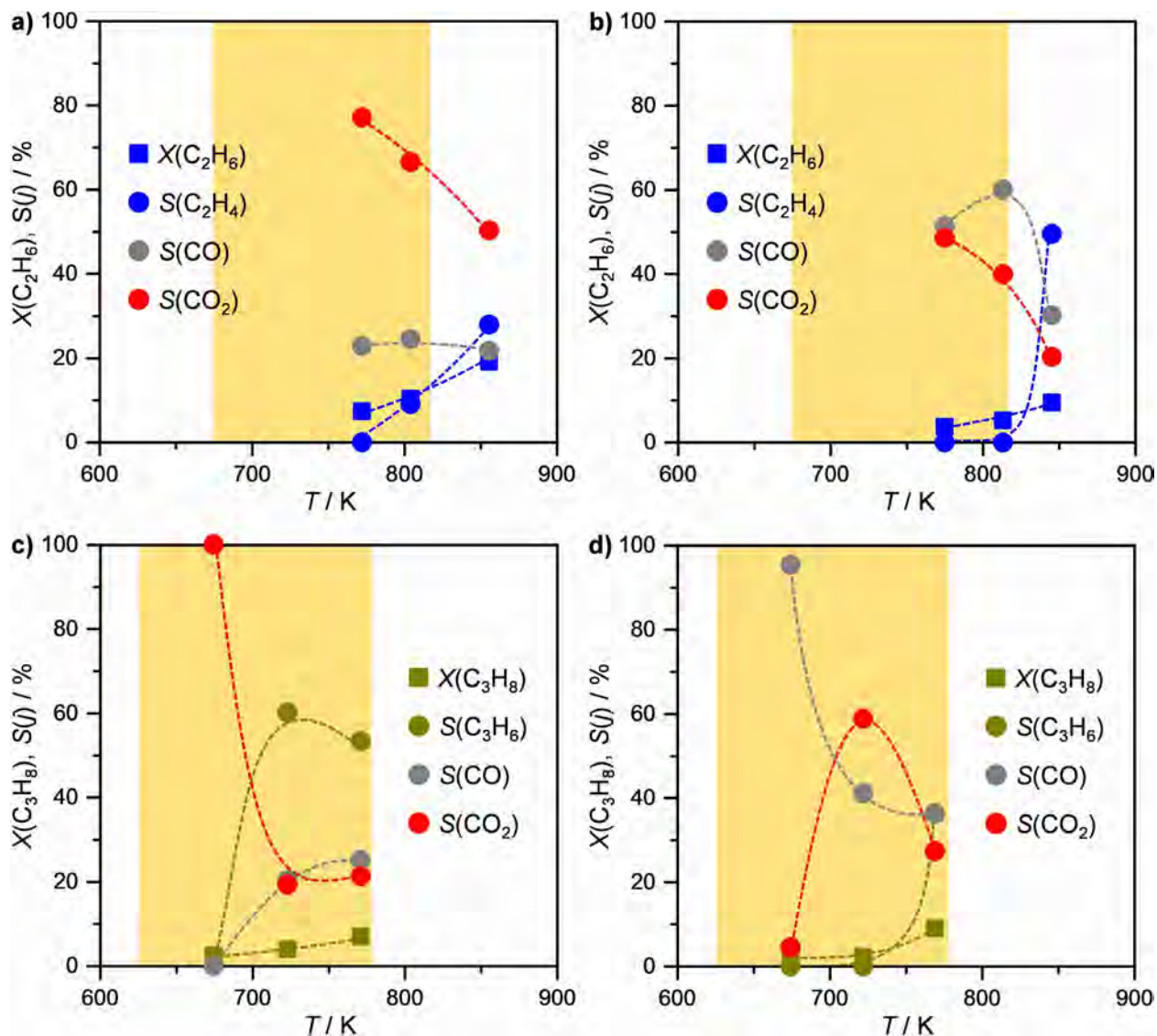
**Figure S9.** Conversion and selectivity *versus* temperature in the oxidation of **a)**, **b)** ethane and **c)**, **d)**, propane over EuOCl/TiO$_2$-a (left) and EuOCl/SiC (right). The yellow boxes denote the operating window of the presented catalytic technology. It can be observed that the combustion and the oxidative dehydrogenation of the alkane over the catalysts is not significant in the operating window of alkane oxychlorination.
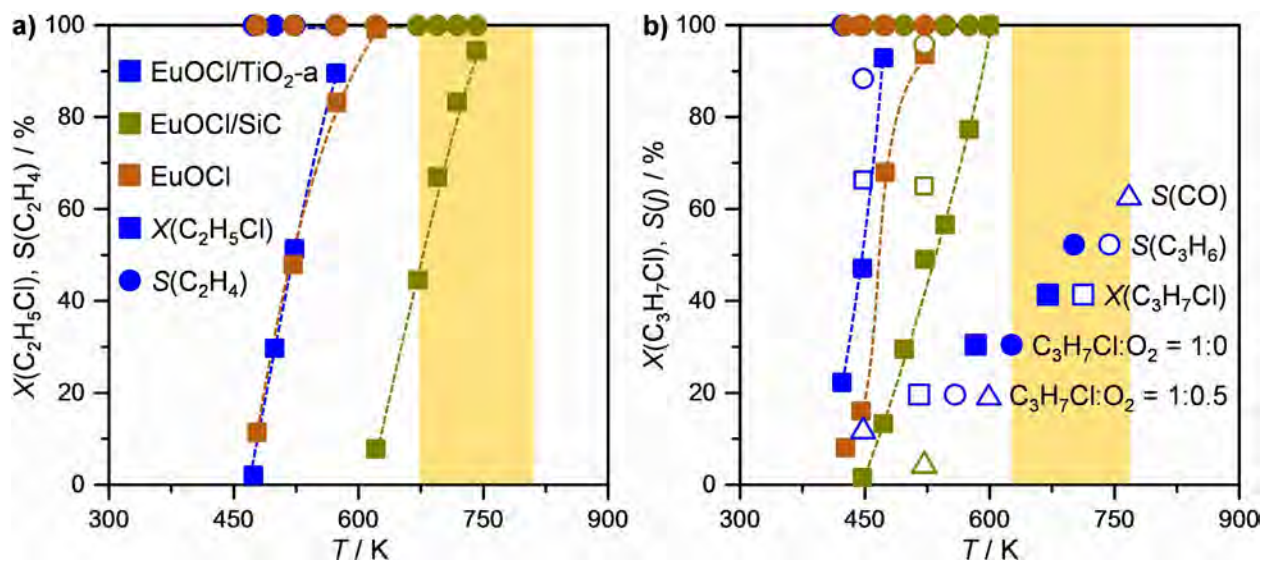
Figure S10. Conversion and selectivity *versus* temperature in the dehydrochlorination of **a)** C_2H_5Cl and **b)** C_3H_7Cl over EuOCl/TiO$_2$-a, EuOCl/SiC, and EuOCl. The yellow boxes denote the operating window of the presented catalytic technology. It can be observed that the light-off curve for alkyl chloride dehydrochlorination over EuOCl/TiO$_2$-a is very similar compared to bulk EuOCl. Instead, over EuOCl/SiC the light-off curve is shifted to higher temperatures, particularly in the case of C_2H_5Cl, where it overlaps with the operating window of ethane oxychlorination. No such overlapping is observed for C_3H_7Cl over the same catalyst, likely due to the higher reactivity of this chlorinated hydrocarbon. Oxygen was also introduced (open symbols) in **b)** to assess the tendency of the supported catalysts to oxidize C_3H_7Cl. In both cases, the C_3H_5Cl conversion raised from 50% to 65%, but the increase occurred at *ca.* 80 K lower temperature over EuOCl/TiO$_2$-a. Moreover, a higher selectivity to CO was observed over EuOCl/TiO$_2$-a compared to EuOCl/SiC (12% and 4%, respectively), indicating that the latter is less prone towards the combustion of the propyl chloride intermediate. The higher level of inertness of the EuOCl/SiC catalyst together with its relatively high ability to selectively dehydrochlorinate C_3H_7Cl in the presence of oxygen and its low tendency to combust propane (**Figure S9d**) might explain the exceptional performance of this catalyst in POC. On the other hand in EOC, the lower reactivity of C_2H_5Cl calls for a more active catalyst. The low tendency towards ethane combustion (**Figure S9a**) and its exceptional activity in C_2H_5Cl dehydrochlorination makes EuOCl/TiO$_2$-a a much better catalyst for ethylene production.

Figure S11. Scanning transmission electron microscopy (STEM) in high-angle annular dark field mode (HAADF) with elemental mapping by means of energy-dispersive X-ray (EDX) of the EuOCl/TiO$_2$-a extrudates **a)** prior to, and **b)** after the oxychlorination of ethane. Elemental color code: Eu: green; Ti: red.
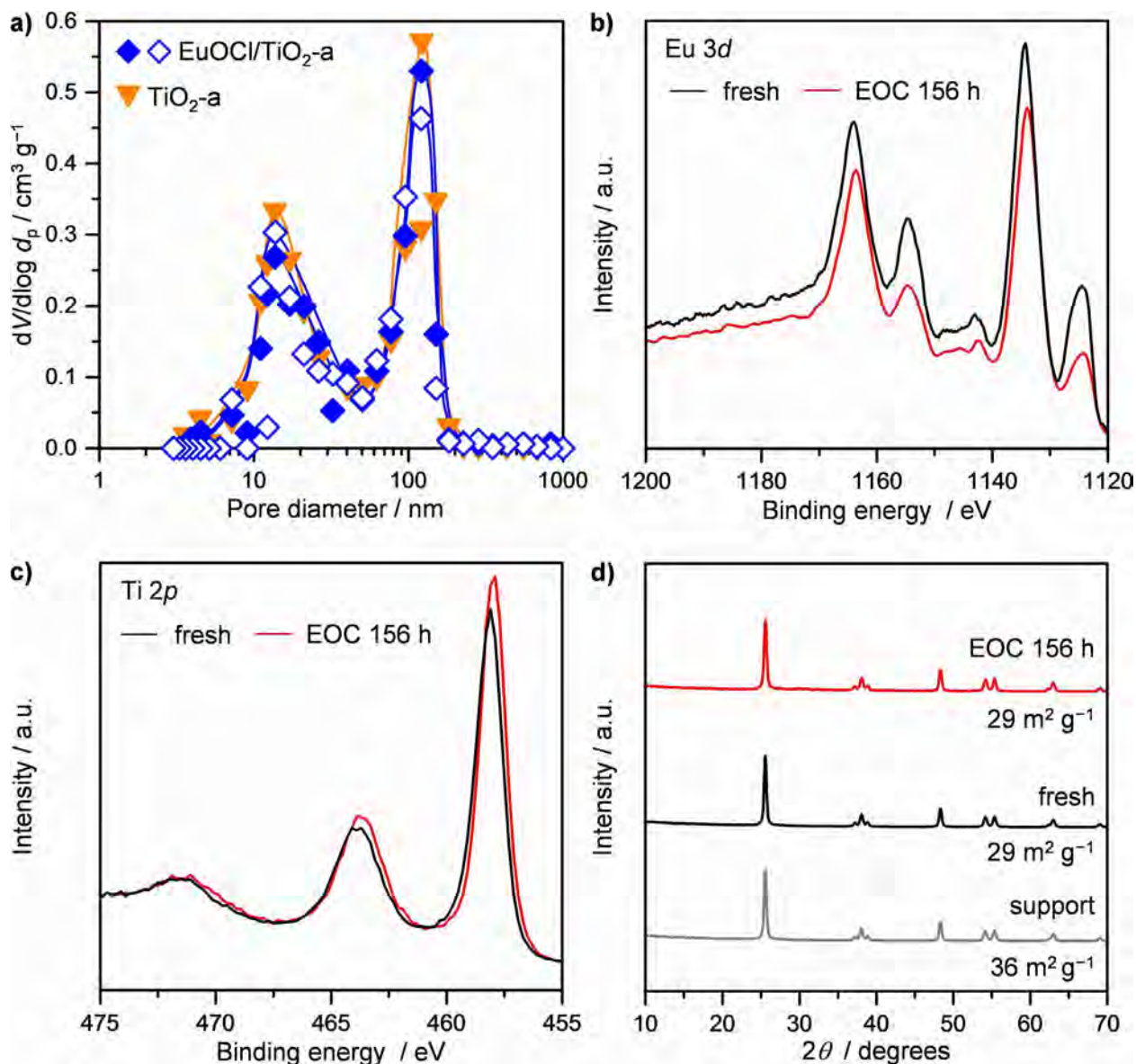
Figure S12. Characterization of the EuOCl/TiO$_2$-a catalysts in extrudate form prior to (fresh) and after the long run showed in **Figure 4f** of the paper. **a)** Pore size distribution of TiO$_2$-a (triangle), and fresh (solid diamond) and used (open diamond) EuOCl/TiO$_2$-a extrudates, derived from mercury porosimetry. **b)** Eu 3d, **c)** Ti 2p core level spectra of fresh (black) and used (red) EuOCl/TiO$_2$-a extrudates. **d)** X-ray diffractograms and total surface area of the TiO$_2$-a support and EuOCl/TiO$_2$-a catalysts in extrudate form prior to (fresh) and used (red).